Dynamics of Bose-Einstein condensates under the influence of periodic and harmonic potentials

N. Hawk Berry and J. Nathan Kutz
Department of Applied Mathematics, University of Washington, Seattle, Washington 98195, USA
(Received 28 August 2006; published 23 March 2007)

A variational method is developed to describe the dynamics of a Bose-Einstein condensate (BEC) trapped in an applied external potential consisting of both a harmonic and periodic component. Using this variational method, the BEC dynamics is shown to be well approximated by four coupled nonlinear differential equations, which describe the fundamental interactions in the system arising from the interplay of amplitude (width), chirp, center position, and center frequency. The simplified analytic theory allows for an efficient and convenient method for characterizing the experimental BEC behavior when localized condensates are generated. It further gives the critical strength ratio of harmonic to periodic potential necessary to support multiple stable lattice sites for the condensate and demonstrates that there can be an underlying chaotic behavior in the condensate system.

DOI: 10.1103/PhysRevE.75.036214 PACS number(s): 82.40.Bj, 03.75.Kk, 03.75.Lm

I. INTRODUCTION

In recent years a large number of research groups across the world have generated Bose-Einstein condensates (BECs) by bringing various dilute gases to extremely low temperatures via laser and evaporative cooling methods (see Ref. [1] and references therein). Much of the resulting BEC research has been aimed at exploiting, manipulating, and characterizing macroscopic quantum phenomena [1,2]. Indeed, BECs have been used to study such diverse phenomena as phase coherence [3–5], matter-wave diffraction [6], quantum logic [7,8], matter-wave transport [9], matter-wave gratings, and pulsed matter-wave lasers [10]. In this paper, we consider the dynamical evolution of the BEC and how to manipulate and control it subject to the influence of both harmonic and periodic trapping potentials [3,4]. Specifically, we apply a variational method [11,12] to the governing nonlinear partial differential equation, which reduces the BEC dynamics to a much simpler set of four coupled nonlinear differential equations, which capture the amplitude, chirp, center position, and center-frequency fluctuations observed in simulations and experiment.

The international proliferation of BEC experiments demonstrates the continued fundamental interest in the applications associated with macroscopic quantum phenomena. In general, repulsive condensates have been shown to be experimentally stable and have lifetimes on the order of seconds to minutes [3]. In contrast, attractive condensates have proven to be more difficult to control and have been shown to collapse in three dimensions [13]. However, the attractive condensates in the quasi-one-dimensional [14] setting are predicted to be stable and robust [14,15]. A Feshbach resonance can be used to efficiently tune the BEC between attractive and repulsive condensates [16]. Indeed, the technology for generating attractive or repulsive BECs is becoming, relatively speaking, commonplace. As such, the ability to control and manipulate the condensate has now become a central issue in the study of BEC matter waves. With regards to periodic potentials, the trapping of the condensate in numerous lattice sites (or troughs of the potential) is of fundamental interest. Our analysis characterizes the dynamic transition from trough to trough and further predicts when multiple lattice sites are stable. The analysis also suggests how to selectively move the condensate from one lattice site to another by simply manipulating the relative strength of the periodic potential.

The paper is outlined as follows: In Sec. II, the governing mean-field equations are presented. Section III develops the variational method and derives the reduced set of four coupled nonlinear differential equations, which govern the system. Sections III A–III C provide extensive theoretical predictions for various cases of the applied potential. The concluding subsection provides the general theory when the BEC is subject to both harmonic and periodic potentials. Section IV builds on the theory of the preceding section to propose methods for controlling and manipulating the condensate. A comparison is also provided with experiment in Sec. V before concluding the paper in Sec. VI with a review of the key results.

II. GOVERNING EQUATIONS

It has been well established that in cigar-shaped BEC trap geometries the macroscopic description of the BEC wave function can be theoretically described by the nonlinear Schrödinger equation with external potential $V(x)$ [14] (Gross-Pitaevskii equation [17,18]),

$$i\psi_t + \frac{1}{2}\psi_{xx} + \alpha|\psi|^2\psi - V(x)\psi = 0. \tag{1}$$

The evolution of the normalized complex-valued mean-field variable $\psi(x,t)$ is derived under the Hartree-Fock approximation [19] in the dilute gas limit [20]. And although much of the work here focuses on attractive BECs ($\alpha=1$), the variational method presented can be used to describe repulsive condensates ($\alpha=-1$) as well (see. Sec. V). Note that for physical potentials, the function $V(x)$ is real.

The specific potential considered here is comprised of both a harmonic and periodic potential [3,4]. Thus the potential $V(x)$ in Eq. (1) is given by

$$V(x) = V_0 \sin^2[\omega(x-\bar{x})] + V_1 x^2, \tag{2}$$

where V_0 and V_1 measure the relative strengths of the periodic and harmonic potentials, respectively. The parameter $\bar{x}$

measures the offset of a minimum of the periodic potential with respect to the minimum of the harmonic potential. Note that if $\bar{x}=\pm n\pi/\omega$, where n is an integer, then a minimum of the periodic potential aligns with the minimum of the harmonic potential.

In the case that $V(x)=0$, the governing equation (1) reduces to the nonlinear Schrödinger equation for which soliton solutions are known to exist [21]. The one-soliton solution is of fundamental interest in BEC theory, water waves [22], plasmas [23], and nonlinear optics [24,25]. Specifically, the stability and dynamics of the one-soliton solution plays a critical role in determining the behavior in such systems. Thus perturbations to the one-soliton solution provide significant insight into the dynamics of a given physical system. Two standard methods have been developed to characterize the behavior of the one-soliton under perturbation: soliton perturbation theory [26] and the variational method [27]. Unfortunately, standard soliton pertubation theory is incapable of reproducing the dynamics observed in the numerical simulations considered here since it fails to capture the quadratic phase changes, which drive the amplitude-width fluctuations. However, the variational method generally provides a quantitative characterization of the dynamics.

III. VARIATIONAL DYNAMICS

Although full simulations are essential to understanding Eq. (1), they often do not give the desired intuition and insight into the fundamental dynamics driving the governing system. Here we extend the variational method, which has been used extensively for Hamiltonian systems. Beginning with the work of Anderson [28], the literature regarding variational reductions in nonlinear Schrödinger-type systems is vast, especially given its applicability in optical transmission systems. Here, we refer the reader to a review article [29] that highlights its many applications and references.

For the system governed by Eq. (1) with Eq. (2) the Lagrangian density [27] is given by

$$\mathcal{L}=i\left(\psi\frac{\partial\psi^*}{\partial t}-\psi^*\frac{\partial\psi}{\partial t}\right)+\left|\frac{\partial\psi}{\partial x}\right|^2-\alpha|\psi|^4+2V(x)|\psi|^2, \quad (3)$$

where $\delta\mathcal{L}/\delta\psi^*=0$ reproduces the governing equation (1). To simplify the following calculations, we assume a Gaussian ansatz. The specific choice of ansatz makes only a small quantitative difference [30] since the integrals to be evaluated below will change only slightly. The ansatz assumption is then

$$\psi=A\sqrt{\eta}\exp(-\eta^2(x-x_0)^2+i[\beta(x-x_0)^2+\xi(x-x_0)+\phi]), \quad (4)$$

where the parameters η, β, x_0, ξ, and ϕ vary with time t and measure the amplitude, quadratic phase (chirp), center position, center frequency, and absolute phase, respectively. The scaling constant A determines the total number of condensed atoms in the trap since $\int_{-\infty}^{\infty}|\psi|^2dx=A^2\sqrt{\pi/2}$.

The ansatz (4) gives a localized BEC solution. Of practical physical interest is the width of the localized solution in relation to the period of the applied sinusoidal potential in Eq. (2). The case considered here, and for which the variational method provides a good approximation, assumes that the frequency of the periodic potential ω in Eq. (2) is small in relation to the amplitude-width parameter η in Eq. (4), i.e., $\omega/\eta\ll 1$. Figure 1 demonstrates the possible parameter regimes that can be considered. The top panel ($\omega/\eta=0.2$) is of interest here since the localized solution can be trapped at the troughs of the periodic potential. The middle panel ($\omega/\eta=4$) and bottom panel ($\omega/\eta=20$) consider the cases when the width of the condensate spans 2–3 troughs or 10–15 troughs, respectively. Numerical simulations of these regimes show that the condensate structure no longer retains the localized solution form (4). Rather, oscillations develop on the envelope of the condensate.

The average Lagrangian [27,29] $L=\int_{-\infty}^{\infty}\mathcal{L}dx$ can now be calculated using the ansatz (4) with (3). Applying the Euler-Lagrange formulas $\delta L/\delta p=0$, where p is one of the parameters η, β, x_0 and ξ gives the reduced dynamical system

$$\frac{d\eta}{dt}=-2\eta\beta, \quad (5a)$$

$$\frac{d\beta}{dt}=2(\eta^4-\beta^2)-\frac{A^2\sqrt{2}}{2}\eta^3-V_0\omega^2\cos[2\omega(\bar{x}-x_0)]-V_1, \quad (5b)$$

$$\frac{dx_0}{dt}=\xi, \quad (5c)$$

$$\frac{d\xi}{dt}=-2V_1x_0+V_0\omega\sin[2\omega(\bar{x}-x_0)], \quad (5d)$$

where we take $\alpha=1$ in Eq. (3) and the right-hand side of Eqs. (5b) and (5d) have been simplified by assuming that $\omega/\eta\ll 1$ so that $\exp[-\omega^2/(2\eta^2)]\approx 1$. This assumption holds in the case that the localized solution is more narrow than the period of the potential, i.e., the case of interest here (see the top panel of Fig. 1). This simplification allows us to extend recent results [11,12] since stability can be computed explicitly. This 4×4 nonlinear system of differential equations governs the interaction between the amplitude, chirp, center position, and center frequency. It should be noted that the inclusion of the chirp is critical since it is the only dynamical quantity that couples with the amplitude as seen in Eq. (5a), thus allowing for amplitude fluctuations. This should be contrasted with soliton perturbation theory, which does not allow for chirp dynamics and therefore disallows amplitude fluctuations for any real potentials $V(x)$. Further, note that the absolute phase variable $\phi(t)$ plays no role in the dynamics (5) due to the phase invariance of Eq. (1). Regardless, $\phi(t)$ can be computed from the equation derived from $\delta L/\delta\phi=0$.

The standard treatment of coupled, nonautonomous nonlinear differential equations involves locating their fixed points and determining their linear stability properties [31]. This often allows the behavior of the global dynamics to be understood based upon the behavior (flow) near the fixed points [28]. Fixed points for Eq. (5) are found where $\beta=\xi=0$ and the following 2×2 system is satisfied for η and x_0:

$$2\eta^4 - \frac{A^2\eta^3}{\sqrt{2}} - V_0\omega^2\cos[2\omega(\bar{x}-x_0)] - V_1 = 0, \tag{6a}$$

$$2V_1x_0 - V_0\omega\sin[2\omega(\bar{x}-x_0)] = 0. \tag{6b}$$

The solutions to these equations are denoted η_0 and X_0. The linear stability of the fixed points $(\eta,\beta,x_0,\xi)=(\eta_0,0,X_0,0)$ is established by considering the evolution of the perturbed quantities denoted by tildes [31]: $\eta=\eta_0+\tilde{\eta}$, $\beta=0+\tilde{\beta}$, $x_0=X_0+\tilde{x}$, and $\xi=0+\tilde{\xi}$. Inserting these into Eq. (5) results in the linearized evolution system

$$\frac{d\mathbf{u}}{dt} = \mathbf{M}\mathbf{u} \rightarrow \mathbf{M}\mathbf{v} = \lambda\mathbf{v}, \tag{7}$$

where the vector $\mathbf{u}=(\tilde{\eta},\tilde{\beta},\tilde{x_0},\tilde{\xi})^T$, the matrix $\mathbf{M}$ is determined from the linearization process [31], and $\mathbf{u}=\mathbf{v}\exp(\lambda t)$. Thus it only remains to compute the eigenvalues of the matrix $\mathbf{M}$ and stability can be determined. If any eigenvalue has a real part greater than zero, the solution is considered unstable. Of course, for the general 4×4 system (5), a simple phase-plane portrait is not possible as it is in the 2×2 case. Rather, a complicated four-dimensional flow is generated, which has the possibility of producing chaotic behavior [31].

For the specific dynamical system considered here, the linearization about the steady-state solution gives the matrix $\mathbf{M}$,

$$\mathbf{M} = \begin{bmatrix} 0 & 1 & 0 & 0 \\ -2V_1 - 2\omega^2V_0\cos\theta & 0 & 0 & 0 \\ 0 & 0 & 0 & -2\eta_0 \\ -2\omega^3V_0\sin\theta & 0 & 8\eta_0^3 - \frac{3\sqrt{2}}{2}A^2\eta_0^2 & 0 \end{bmatrix}, \tag{8}$$

where $\theta=2\omega(\bar{x}-X_0)$. The eigenvalues of this matrix can be calculated analytically. The four roots λ_j $(j=1,2,3,4)$ are calculated from two quadratic equations,

$$\lambda_{1,2} = \pm i\sqrt{16\eta_0^4 - 3\sqrt{2}A^2\eta_0^3}, \tag{9a}$$

$$\lambda_{3,4} = \pm i\sqrt{2V_1 + 2\omega^2V_0\cos\theta}. \tag{9b}$$

If the quantities under the radicals of the square root are positive, then the corresponding fixed point is orbitally stable [31]. For the Hamiltonian system considered here, this is the best one can expect from the linear stability. However, if either of the quantities in the square root is negative, then a saddle structure is expected and the fixed point is unstable.

With no applied potential $(V_1=V_0=0)$, the evolution of the center position and center frequency is trivial. By Noether's theorem [33], the translational and Galilaen invariance of the system [32] require two of the four eigenvalues (9) to be zero, i.e., $\lambda_{3,4}=0$. In contrast, the chirp and amplitude interact to generate nontrivial dynamics similar to those considered in dispersion-managed optical systems [30]. The chirp-amplitude interaction can be characterized by considering the fixed points of the system, which occur for $\beta=0$ and when Eq. (6a) reduces to $\eta^3(\eta-A^2\sqrt{2}/4)=0$. Thus there are two fixed points: $\eta_0=0$ and $\eta_0=A^2\sqrt{2}/4$. The primary interest is in real and positive η_0 due to the physical consideration of the form of ansatz chosen in Eq. (4). Linearizing about η_0 we find the two remaining eigenvalues of Eq. (9) to be $\lambda_{1,2}=\pm iA^4/4$. Purely oscillatory behavior occurs since the eigenvalues have no real part. The fixed point at $\eta=0$ is a degenerate point for which a standard linear stability analysis yields no information [30]. Thus the center-point is surrounded by a separatrix, which emanates and terminates at the origin, showing that for initial chirp-amplitude values, which lie within the separatrix, periodic breathing dynamics will ensue.

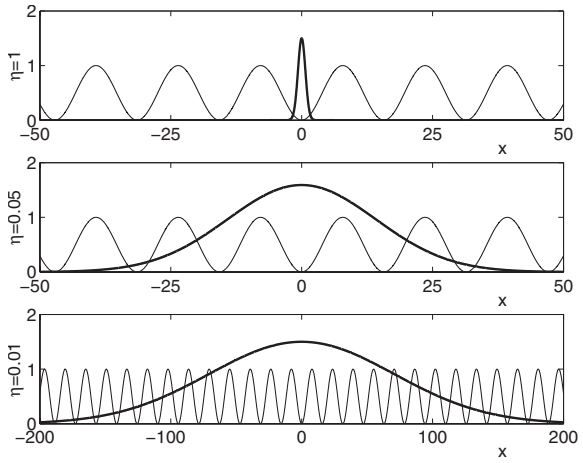

FIG. 1. Localized condensate (bold line) and applied periodic potential (light line) for $\omega/\eta=0.2,4$, and 20 (top, middle, and bottom panels, respectively). Here we choose $\omega=0.2$ in Eq. (2) and the parameter A in Eq. (4) so that the amplitude of the condensate is 1.5. The value of η is given on the left of each panel. The case of physical interest is represented in the top panel.

A. No periodic potential: $V_0=0$

In the absence of a periodic potential, the harmonic potential determines the dynamics. In this case, Eq. (5) shows that the amplitude-chirp dynamics separate from the center-position and center-frequency dynamics resulting in two 2×2 systems. It should be noted that the assumption $\omega/\eta\ll1$ in Eq. (5) is irrelevant to the dynamics presented in this section. The center-position and center-frequency equations (5c) and (5d) are linear and can be solved exactly giving only oscillatory behavior for the center-position and center-frequency $(\lambda_{3,4}=\pm i\sqrt{2V_1})$.

The amplitude-chirp dynamics follow closely from the previous subsection with the notable exception that the parameter V_1 is now included. Fixed points are found for $\beta=0$ and when Eq. (6a) reduces to

$$2\eta^4 - \frac{A^2}{\sqrt{2}}\eta^3 - V_1 = 0. \tag{10}$$

The only solutions of interest are those roots of Eq. (10) that are real and positive. This restriction comes from the physical consideration of the form of ansatz chosen in Eq. (4). For

a root η_0, which is real and positive, we find that by using Eq. (6a) the eigenvalues of Eq. (9) are

$$\lambda_{1,2} = \pm i\sqrt{8V_1 + \eta_0^3 A^2\sqrt{2}}, \tag{11}$$

where we recall that $V_1 > 0$ for the confining potential considered here. Thus again the behavior of the amplitude-chirp interaction is oscillatory.

B. No harmonic potential: $V_1 = 0$

The periodic potential gives rise to a more complex phase plane and interaction dynamics. In this case, all four parameters in Eq. (5) remain coupled with the amplitude-chirp dynamics slaved to the center-position and center-frequency dynamics. Further, the quality of the variational approximation relies now on $\omega/\eta \ll 1$. Indeed, large fluctuations in η can compromise the agreement with Eq. (1). Fixed points are found for $\beta = \xi = 0$. The nonlinear algebraic equations (6a) and (6b), which must also be satisfied, reduce to

$$2\eta^4 - \frac{A^2}{\sqrt{2}}\eta^3 - V_0\omega^2 \cos\theta = 0 \quad \text{and} \quad \sin\theta = 0. \tag{12}$$

In order for the second equation to be satisfied, we require θ to be a multiple of π so that $X_0 = \bar{x} - (n\pi)/(2\omega)$, where $n = 0, \pm 1, \pm 2 \ldots$. This then reduces Eq. (12) to

$$2\eta^4 - \frac{A^2}{\sqrt{2}}\eta^3 - (-1)^n V_0\omega^2 = 0. \tag{13}$$

Note that for $n = 0, \pm 2, \pm 4 \ldots$, i.e., when we are at a trough of the periodic potential, $V_0\omega^2 > 0$ takes on the same role as V_1 in the harmonic potential in the previous subsection. And for $n = \pm 1, \pm 3 \ldots$ there is a sign change. This sign change is critical in determining the stability of the fixed points. Equation (13) produces four roots, only two of which are real. And of these two, only positive ones are of physical interest. Specifically, the triple root at the origin bifurcates into two complex roots and one nonzero, real root. Thus depending on the specific parameter regime chosen, we can either have one or two roots for which $\eta_0 > 0$.

The stability of the fixed points can be determined from Eq. (9). Specifically, rewriting Eq. (9a) using Eq. (6a) and the fact that $V_1 = 0$ gives

$$\lambda_{1,2} = \pm i\sqrt{\sqrt{2}A^2\eta_0^3 + \omega^2 V_0 \cos\theta}, \tag{14a}$$

$$\lambda_{3,4} = \pm i\sqrt{2\omega^2 V_0 \cos\theta}. \tag{14b}$$

These expressions lead to very simple conclusions: if we are in a trough of the periodic potential so that $n = 0, \pm 2, \pm 4 \ldots$, then $\cos\theta = 1$ and both $\lambda_{1,2}$ and $\lambda_{3,4}$ are purely imaginary since the quantities under the square roots are strictly positive. Recall that we are assuming $V_0 > 0$ and $V_1 > 0$. In contrast, if we are on the peak of a potential so that $n = \pm 1, \pm 3 \ldots$, then $\cos\theta = -1$ and Eq. (14b) leads to saddle behavior since the eigenvalues $\lambda_{3,4}$ are now real with one being positive and one being negative. The remaining pair of eigenvalues is purely imaginary since they reduce to $\lambda_{1,2} = \pm i\sqrt{4\eta_0^4 + \omega^2 V_0}$, where the quantity in the square root is always strictly positive.

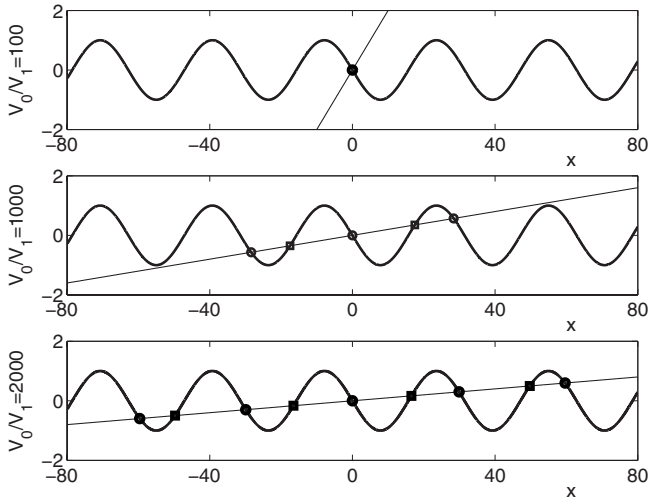

FIG. 2. Graphical representation of the birth of fixed points as a function of the parameter V_0/V_1 for $\omega = 0.1$ and $\bar{x} = 0$. The light lines are the left side of Eq. (15) and the bold lines are the right side of Eq. (15). Note that as V_0/V_1 is increased, pairs of fixed points (saddle-center pairs) are created symmetrically about the origin. The stable centers are indicated with circles, whereas the unstable saddles are denoted by squares.

C. Harmonic and periodic potentials

We now consider the full dynamics, which include both the harmonic and periodic potentials. To begin, we consider Eq. (16b), which determines the x position of the fixed points X_0. This gives the relation

$$\frac{2V_1}{\omega V_0} X_0 = \sin\theta. \tag{15}$$

As V_0 is increased relative to V_1, pairs of fixed points are created. A graphical representation of the birth of the fixed-point pairs as a function of increasing V_0 is shown in Fig. 2.

Once the fixed points are calculated numerically from the transcendental equation (15), they can be used in Eq. (6a) to solve for η_0. Stability can then be established by solving for the eigenvalues (9). We rewrite the expressions for the eigenvalues using Eq. (6) as

$$\lambda_{1,2} = \pm i\sqrt{A^2\sqrt{2}\eta_0^3 + V_1\left(1 + \frac{\omega^2 V_0}{V_1}\cos\theta\right)}, \tag{16a}$$

$$\lambda_{3,4} = \pm i\sqrt{2V_1\left(1 + \frac{\omega^2 V_0}{V_1}\cos\theta\right)}. \tag{16b}$$

This illustrates the importance of the ratio $\omega^2 V_0/V_1$. In particular, for $\omega^2 V_0/V_1 < 1$, the eigenvalues are always purely imaginary since the quantities under the square root are strictly positive. However, once $\omega^2 V_0/V_1 > 1$, the values of λ_3 and λ_4 can alternate between purely imaginary (stable center) and purely real (unstable saddle) as $\cos\theta$ oscillates between positive and negative values as a function of X_0. Figure 2 illustrates the creation of fixed points as a function of the parameter $\omega^2 V_0/V_1$. Indeed, the following two important graphical observations can be made concerning the cre-

ated fixed points to the right of the origin: one of the fixed points resides in quadrant III, where $\theta \in [\pi, 3\pi/2]$, which gives purely real eigenvalues (unstable saddle) for Eq. (16b) since $\cos\theta < 0$. In contrast, the second created fixed point resides in quadrant IV, where $\theta \in [3\pi/2, 2\pi]$, so that $\cos\theta > 0$ and the eigenvalues (16) are purely imaginary (stable center). Thus the fixed points are created in saddle-center pairs as a function of increasing $\omega^2 V_0/V_1$. Similar observations can be made for the fixed points to the left of the origin. In this case, however, the fixed points are in quadrants II and I, respectively, so that the sign argument presented above is preserved.

For the sake of simplifying the above argument, we assume that a minimum of the periodic potential is aligned with the minimum of the harmonic potential so that $\bar{x}=0$. Then $X_0=0$ is a solution. Indeed, this is the only solution for $V_0 \ll V_1$. Essentially, the harmonic potential dominates the BEC dynamics in this parameter regime. However, as V_0 is increased relative to V_1, pairs of fixed points are created symmetrically on either side of $x=0$ (see Fig. 2), and in the limit $V_1/V_0 \to 0$, there are an infinite number of fixed points as given in Sec. III B.

As a consequence of the interaction between the harmonic and periodic potentials, only a finite number of fixed points are possible for a given strength of the two potentials. The exact number is determined by the quantity $\omega^2 V_0/V_1$. A large number of stable lattice sites requires the periodic potential to be much larger than the harmonic potential ($V_0 \gg V_1$). Alternatively, only the minimum of the harmonic well is stable for $\omega^2 V_0/V_1 < 1$. Figures 3–6 exemplify the typical dynamics, which can result in the system when three stable fixed points are present. In this series of four figures, we choose $V_0/V_1=1000$ with $\omega=0.1$, which corresponds to the middle panel of Fig. 2. Thus the three stable (center) fixed points are located at $x_0=0$ and $x_0 \approx \pm 28$. Figure 3 demonstrates the dynamics of Eq. (5) near the fixed point at the origin. Note that the amplitude and chirp exhibit a beating-type phenomenon, which results from the interaction of the two frequencies (16) in the system: the frequency of center-position fluctuations and the frequency of the amplitude-chirp oscillations. Likewise, Fig. 4 demonstrates the dynamics of the condensate trapped in the neighboring stable (center) lattice site. Here the oscillatory structure is more complicated since the fixed point is no longer at the minimum of the harmonic potential so that an asymmetry in the dynamics arises. This asymmetry can be seen by comparing the three-dimensional phase portraits in Figs. 3 and 4. Note that the bottom panels of both Figs. 3 and 4 also provide a direct comparison of the governing evolution dynamics (1) with Eq. (2) and the variational approximation (5). Remarkably good agreement is achieved.

The final figures, Figs. 5 and 6, demonstrate the typical behavior that occurs for an initial displacement x_0 well beyond any of the stable fixed points. In this case, the condensate simply slides over all the fixed points as it oscillates in the harmonic trap. The phase-plane structure demonstrated in Fig. 5 is characteristic of this parameter regime. Furthermore, the sensitive dependence of the evolution upon the initial conditions is demonstrated, which establishes the chaotic nature of the system. In many respects, the resulting chaos in the system is much like that of the forced Duffing oscillator [31]. Figure 6 shows strong fluctuations in amplitude and position, and although it does not show an exceptional quantitative agreement, the strong breathing behavior is qualitatively well captured by the variational approximation. Part of the reason for this discrepancy is the sensitivity of the evolution to the initial data (chaotic behavior), which makes a quantitative comparison between Eq. (1) with Eqs. (2) and (5) difficult.

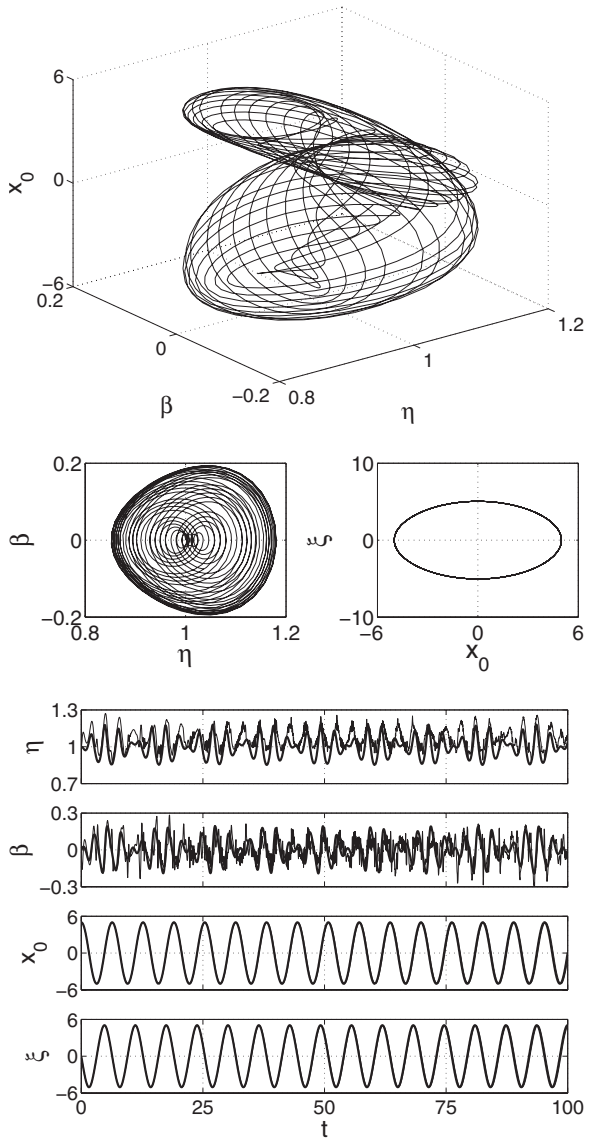

FIG. 3. Phase-plane dynamics of Eqs. (5). The top figure shows a three-dimensional representation of the dynamics in (η, β, x_0) while the middle two panels project the dynamics onto the η-β plane and the x_0-ξ plane. The bottom set of figures are η, β, x_0, and ξ as a function of time for the governing equations (1) with Eq. (2) (light) and variational approximation (5) (bold). The parameter values are $V_0=50$, $V_1=0.05$, $\omega=0.1$, and $A=1.5$. The initial conditions are $(\eta, \beta, x_0, \xi)=(1, 0, 5, 0)$.

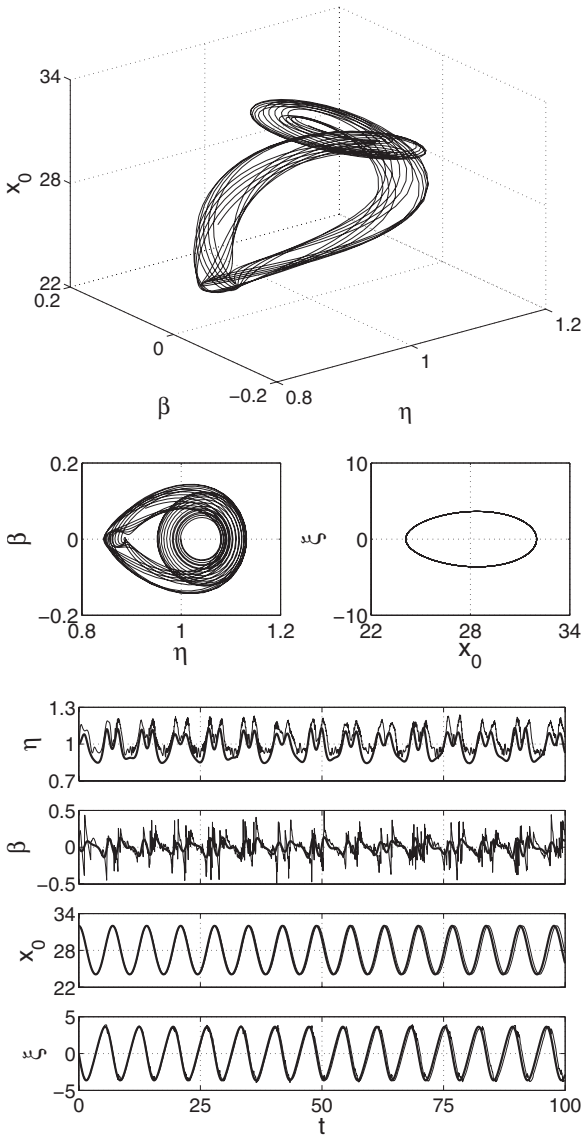

FIG. 4. Phase-plane dynamics of Eqs. (5). The top figure shows a three-dimensional representation of the dynamics in (η,β,x_0), while the middle two panels project the dynamics onto the η-β plane and the x_0-ξ plane. The bottom set of figures are η, β, x_0, and ξ as a function of time for the governing equations (1) with Eq. (2) (light) and variational approximation (5) (bold). The parameter values are $V_0=50$, $V_1=0.05$, $\omega=0.1$, and $A=1.5$. The initial conditions are $(\eta,\beta,x_0,\xi)=(1,0,32,0)$.

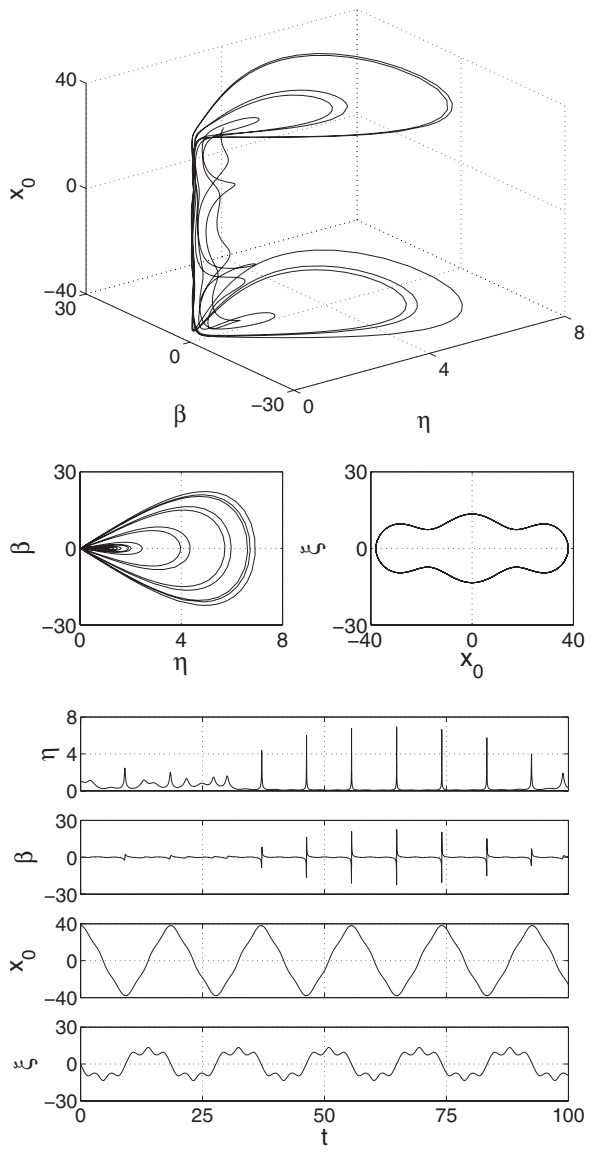

FIG. 5. Phase-plane dynamics of Eqs. (5). The top figure shows a three-dimensional representation of the dynamics in (η,β,x_0), while the bottom two panels project the dynamics onto the η-β plane and the x_0-ξ plane. The bottom set of figures are η, β, x_0, and ξ as a function of time. The parameter values are $V_0=50$, $V_1=0.05$, $\omega=0.1$, and $A=1.5$. The nearly identical initial conditions $(\eta,\beta,x_0,\xi)=(1,0,70,0)$ (solid) and $(\eta,\beta,x_0,\xi)=(1,0,70.2,0)$ (dotted), demonstrate the sensitivity to initial conditions and chaos.

IV. CONTROL OF THE BEC

The previous section establishes that the variational reduction (5) provides a useful, accurate, and greatly simplified description of the governing BEC dynamics given by Eq. (1) with Eq. (2). Indeed, a great deal of analytic progress can be made in understanding the underlying dynamics by making simple connections with the standard theory of phase-plane analysis. Further, the computational time associated with Eq. (5) is orders of magnitude faster than simulations of Eq. (1) with Eq. (2).

The resulting theoretical insight can be used, for instance, to provide information on controlling the BEC dynamics. In the example illustrated in Figs. 7 and 8, the theoretical findings provide both a guide to prescribing the relative strengths of the periodic and harmonic potentials required to achieve three stable fixed points, i.e., $\omega^2 V_0/V_1>1$, and an estimate for the oscillation frequency in the harmonic potential (11) in the absence of a periodic potential. The two together can be used to calculate a specific periodic potential, which can trap the condensate in one of its three stable fixed points. If initially the condensate is near the fixed point to the right of the origin, we can turn off the periodic potential, calculate the half period of oscillation required to move the condensate to the fixed point to the left of the origin [see Eq. (11)], and then turn the periodic potential back on, thus trapping the

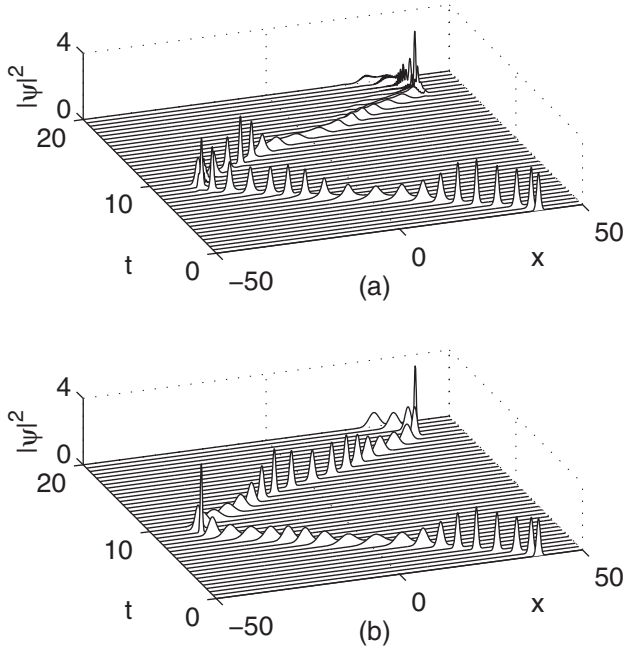

FIG. 6. Evolution of the governing equations (1) with Eq. (2) (top) and variational approximation Eqs. (5) (bottom). The parameter values are $V_0=50$, $V_1=0.05$, $\omega=0.1$, $x_0=38$, $\eta=1$, and $A=1.5$.

condensate two stable fixed points away. The evolution dynamics in this case is demonstrated in Fig. 7. In the phase-plane picture of Fig. 8, the flow of the solution in the reduced variables clearly shows the transfer of the solution from one fixed point to the other.

A wide range of other control experiments can be envisioned and calculated using the simplified variational model (5). Indeed, not only can one perform virtual experiments with Eq. (5) at a fraction of the computational cost of Eq. (1) with Eq. (2), but the analytic results of the previous section allow for simple analytic calculations in which no simulations are required. This allows for the efficient construction and testing of experimental ideas before embarking on extensive and costly computational or experimental studies.

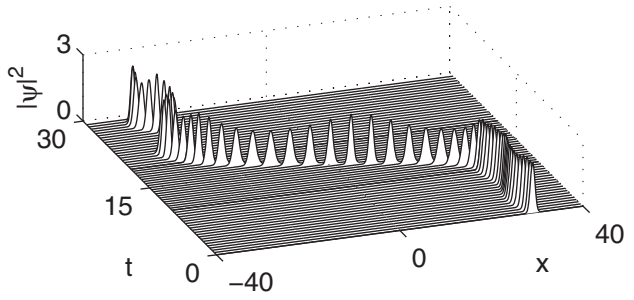

FIG. 7. Evolution of the variational approximation (5) showing the controlled placement of the BEC from one stable fixed point to another. The parameter values assumed are $V_0=50$, $V_1=0.1$, $\omega=0.1$, $x_0=29$, $\eta=1$, and $A=1.5$. At time $t=10$, the periodic potential is turned off so that $V_0=0$. It is turned back on $t=9.2$ time units later thus trapping the condensate near the fixed point on the other side of the origin.

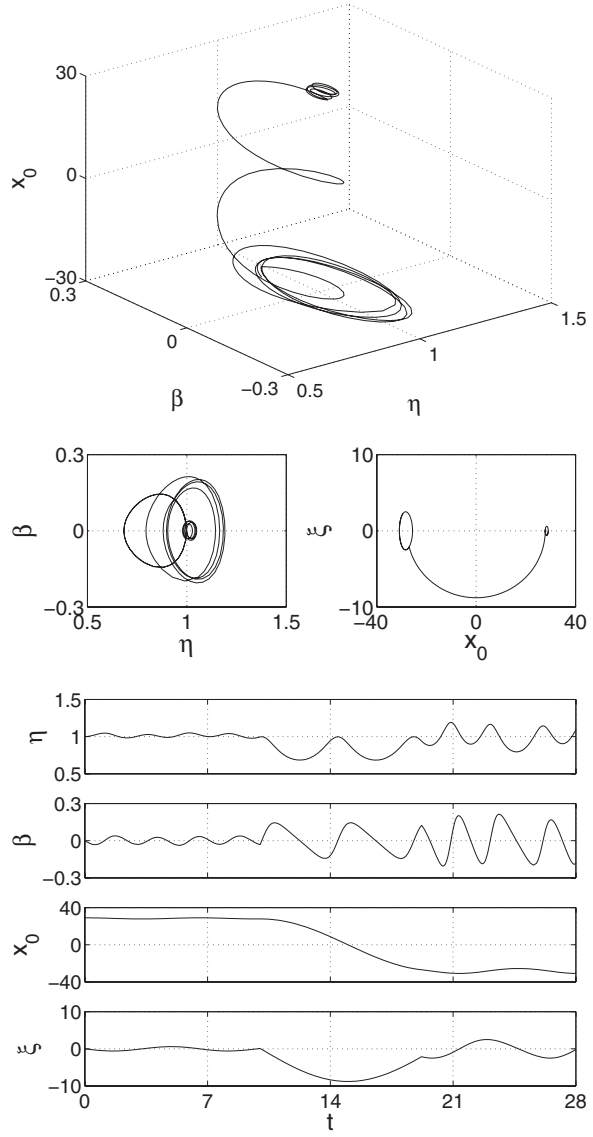

FIG. 8. Phase-plane dynamics of Eqs. (5) with $V_0=50$, $V_1=0.05$, $\omega=0.1$, and $A=1.5$. The top figure shows the dynamics in (η,β,x_0) while the middle panels project the dynamics onto the η-β plane and the x_0-ξ plane. The bottom figures are η, β, x_0, and ξ as a function of time. The initial conditions $(\eta,\beta,x_0,\xi)=(1,0,29,0)$ trap the condensate at the fixed point to the right of $x=0$. At $t=10$, the periodic potential is turned off so that $V_0=0$. It is turned back on $t=9.2$ time units later thus trapping the condensate near the fixed point to the left of $x=0$.

V. COMPARISON WITH EXPERIMENT

Lending support and validity to the variational reduction is a direct comparison to experimental findings. Specifically, Ketterle's MIT group has produced a number of publicly available movies demonstrating their experimental findings [34,35]. We consider a specific animation, which corresponds to the quasi-one-dimensional regime considered here. In the experiment, the BEC is trapped in the defocusing regime so that $\alpha=-1$ in Eq. (1). For data that remains localized, the variational method remains valid in the defocusing regime with Eq. (5b) now becoming

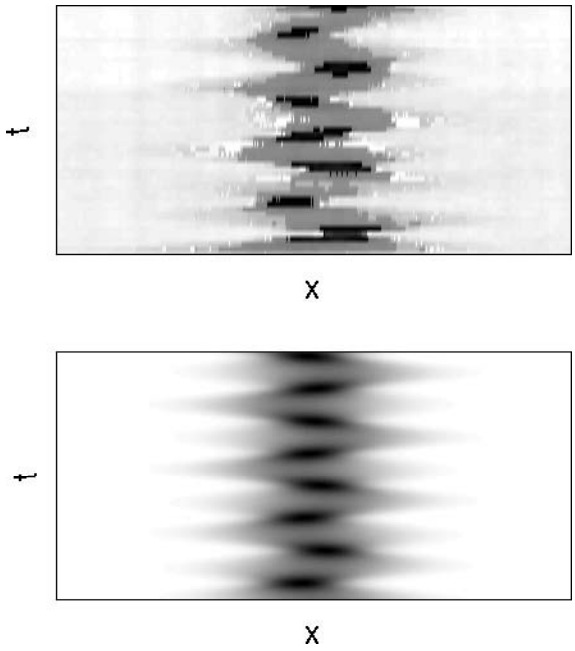

FIG. 9. Comparison of experimental findings (top) with the variational approximation (5) (bottom). The quasi-one-dimensional experiment considered can be found at Ref. [36]. A parameter fit is used to construct the matching theoretical dynamics. Specifically, we take $V_1=0.1$, $V_0=0$, $\omega=0.1$, $A=1.3$ with initial conditions $(\eta,\beta,x_0,\xi)=(0.5,0,0.4,0)$. All the features of the experimental condensate, such as the amplitude fluctuations and center-position oscillations, are well captured with the variational method.

$$\frac{d\beta}{dt} = 2(\eta^4 - \beta^2) + \frac{A^2\sqrt{2}}{2}\eta^3 - V_0\omega^2 \cos\theta - V_1. \quad (17)$$

Thus there is only a sign change to the η^3 term.

To characterize the experimentally measured dynamics of the BEC, we export the experimental movie frames [36] and take a one-dimensional slice in the x direction to capture the spatial profile of the condensate. Further, for visualization purposes, we then take a small segment of time for which the condensate undergoes 7–8 oscillations in the harmonic trap. Figure 9 compares the BEC experimental dynamics with the variational results of Eqs. (5) with Eq. (17). Since we have insufficient experimental data with which to work, i.e., the spatial scales and amplitudes are not clear in the movie, we simply simulate Eqs. (5) with Eq. (17) to approximately fit the experiment. The agreement is remarkably good and all the key features of the experimental condensate, such as the amplitude fluctuations and center-position oscillations, are very nicely captured with the variational approximation. Further, a comment is made by the Ketterle group [36] that the amplitude oscillations eventually die down in time due to natural damping in the experiment, whereas the center-position oscillations continue. Here, the initial conditions generate a small amount of dispersive radiation, which acts much like a damping mechanism since there is a loss of localized condensate. Note that the reduced system (5) does not account for this physical mechanism. However, it is clear from Eqs. (5) that only the amplitude-chirp dynamics depend upon the total number of condensed atoms, which is given by $\int_{-\infty}^{\infty}|\psi|^2dx=A^2\sqrt{\pi/2}$. Regardless, the experimental results confirm the analytic findings that the amplitude, width, and chirp fluctuations are *independent* of, or *decouple* from, the center-position and center-frequency dynamics. This confirms a well-known result for harmonic potentials.

VI. CONCLUDING REMARKS

The continued interest in the dynamics of Bose-Einstein condensates has led to a sustained effort by a large number of groups across the world to manipulate and manage the condensate in a variety of traps. Two of the primary traps used to contain the condensate are of the harmonic and sinusoidal form. In this paper, we have considered the dynamics of the condensate in the presence of these two ubiquitous trapping potentials, and we have shown that the condensate dynamics can be reduced via a variational method to a set of four coupled nonlinear differential equations. This reduced set of equations agrees remarkably well with full numerical simulations and highlights the dominant physical interactions in the system, namely amplitude, width, chirp, center-position, and center-frequency dynamics. Specifically, it provides quantitatively accurate results for the condensate trapped near local troughs in the potential, and for condensates that exhibit both large center-position and amplitude fluctuations, the reduced model provides qualitatively correct behavior. Indeed, quantitative matching is not possible for this case due to the inherently chaotic behavior of the amplitude-chirp dynamics that resembles the forced Duffing oscillator [31].

From a practical point of view, the reduced model provides a highly efficient method for characterizing the control of the condensate subject to harmonic and periodic potentials. It further provides simple analytic results, which provide criteria on the relative strengths of the harmonic and periodic potentials necessary to trap the condensate in local troughs of the periodic potential. Moreover, standard methods of phase-plane analysis determine the frequency of oscillation in the trap as well as the fixed-point locations, thus providing insight into controlling and manipulating the condensate for macroscopic quantum applications [1–10].

ACKNOWLEDGMENTS

We would like to thank Todd Kapitula for useful discussions about the BEC dynamics. We are also indebted to Nicholas Lederer for extracting data from the MIT Ketterle movies for the creation of Fig. 9. N.H.B. acknowledges support from Mary Gates Undergraduate Research and (Grant No. DMS-9810726) and NSF-VIGRE. J. N. Kutz acknowledges support from NSF (Grants No. DMS-0092682 and No. DMS-0604700).

[1] W. Ketterle, D. S. Sturfee, and D. M. Stamper-Kurn, in *Proceedings of the International School of Physics "Enrico Fermi"* (IOS Press, Amsterdam, Washington, D.C., 1999), pp. 67–176.
[2] F. Dalfovo, S. Giorgini, L. P. Pitaevskii, and S. Stringari, Rev. Mod. Phys. **71**, 463 (1999).
[3] B. P. Anderson and M. A. Kasevich, Science **282**, 1686 (1998).
[4] E. W. Hagley, L. Deng, M. Kozuma, J. Wen, K. Helmerson, S. L. Rolston, and W. D. Phillips, Science **283**, 1706 (1999).
[5] M. L. Chiofalo and M. P. Tosi, Phys. Lett. A **268**, 406 (2000).
[6] Y. B. Ovchinnikov, J. H. Muller, M. R. Doery, E. J. D. Vredenbregt, K. Helmerson, S. L. Rolston, and W. D. Phillips, Phys. Rev. Lett. **83**, 284 (1999).
[7] D. Jaksch, C. Bruder, J. I. Cirac, C. W. Gardiner, and P. Zoller, Phys. Rev. Lett. **81**, 3108 (1998).
[8] G. K. Brennen, C. M. Caves, P. S. Jessen, and I. H. Deutsch, Phys. Rev. Lett. **82**, 1060 (1999).
[9] D.-I. Choi and Q. Niu, Phys. Rev. Lett. **82**, 2022 (1999).
[10] L. D. Carr and J. Brand, Phys. Rev. A **70**, 033607 (2004).
[11] J. Brand and A. R. Kolovsky, Eur. Phys. J. D **10**, 1140 (2006).
[12] A. Trombettoni and A. Smerzi, Phys. Rev. Lett. **86**, 2353 (2001).
[13] P. A. Ruprecht, M. J. Holland, K. Burnett, and M. Edwards, Phys. Rev. A **51**, 4704 (1995).
[14] L. D. Carr, M. A. Leung, and W. P. Reinhardt, J. Phys. B **33**, 3983 (2000).
[15] J. C. Bronski, L. D. Carr, R. Carretero-González, B. Deconinck, J. N. Kutz, and K. Promislow, Phys. Rev. E **64**, 056615 (2001).
[16] S. L. Cornish, N. R. Claussen, J. L. Roberts, E. A. Cornell, and C. E. Wieman, Phys. Rev. Lett. **85**, 1795 (2000).
[17] L. P. Pitaevskii, Sov. Phys. JETP **13**, 451 (1961).
[18] E. P. Gross, Nuovo Cimento **20**, 454 (1961).
[19] G. Baym, *Lectures in Quantum Mechanics* (Addison-Wesley, Reading, MA, 1989).
[20] E. H. Lieb and R. Seiringer, Phys. Rev. Lett. **88**, 170409 (2002).
[21] M. Ablowitz and H. Segur, *Solitons and the Inverse Scattering Transforms* (SIAM, Philadelphia, 1981).
[22] H. C. Yuen and B. M. Lake, Adv. Appl. Mech. **22**, 67 (1982).
[23] F. Chen, *Introduction to Plasma Physics and Controlled Fusion* (Plenum, New York, 1984).
[24] R. Boyd, *Nonlinear Optics* (Academic Press, New York, 1992).
[25] G. Agrawal, *Nonlinear Fiber Optics* (Academic Press, New York, 1989).
[26] See, for instance, J. N. Elgin, Phys. Rev. A **47**, 4331 (1993).
[27] G. Whitham, *Linear and Nonlinear Waves* (Wiley-Interscience, New York, 1974).
[28] D. Anderson, Phys. Rev. A **27**, 3135 (1983).
[29] B. A. Malomed, Prog. Opt. **43**, 69 (2002).
[30] J. N. Kutz, P. Holmes, S. G. Evangelides, and J. P. Gordon, J. Opt. Soc. Am. B **15**, 87 (1998).
[31] P. G. Drazin, *Nonlinear Systems* (Cambridge University, Cambridge, England, 1992).
[32] P. G. Drazin and R. S. Johnson, *Solitons: An Introduction* (Cambridge University Press, Cambridge, England, 1990).
[33] I. M. Gelfand and S. V. Fomin, *Calculus of Variations* (Prentice-Hall, Englewood Cliffs, NJ, 1963).
[34] *Standard Mathematical Tables and Formulae*, 30th ed., edited by D. Zwillinger (CRC Press, Boca Raton, 1996).
[35] cua.mit.edu/ketterle_group/animations.htm
[36] cua.mit.edu/ketterle_group/Animation_folder/Oscillations.htm